Internal Model Control of Coupled Distillation Columns

An experimental evaluation of methods to analyze process resilience based on internal model control (IMC) has been performed. A pilot plant consisting of two coupled distillation columns was instrumented for control studies using an LSI 11/23 microcomputer. Two alternative sets of inputs were chosen and the two full 7 (all outputs) $\times$ 4 (all inputs) transfer matrix models of the pilot plant were identified. From these models, a large number of potential 3 $\times$ 3 control structures were first screened for different levels of achievable control performance using the newly developed tools for resilience analysis. Without the need for simulation and with minimal computational effort these new techniques allow prediction of the effect of nonminimum phase characteristics, input constraints, and model uncertainty on achievable closed-loop performance. The resilience analysis results were found to be in agreement with qualitative physical intuition. To more fully investigate the usefulness and precision of the resilience analysis, three control structures for maintaining three product compositions from a distillation system were studied experimentally. The design and performance of IMC for this complex system is demonstrated and compared with single-loop PID controllers combined with a dynamic decoupler.

K. L. Levien, Manfred Morari
Department of Chemical Engineering
University of Wisconsin
Madison, WI 53706

Introduction

The purpose of this paper is to demonstrate the use of recently proposed analytical methods to evaluate the control properties of alternative designs. Such evaluations are important in two general situations: when a choice among physically different processes must be made at the design stage, or when the most appropriate control structure for an already existing process must be selected. As an example of the first situation, the "controllability" evaluation of a process that utilizes heat integration and recycle streams to achieve efficient steady state performance vs. one that does not, is frequently of interest. For the second situation, much of the research on the control of distillation columns has included comparisons of alternate control structures (sets of inputs) for a single equipment configuration.

The integrated nature of modern chemical plants requires that attention be paid to aspects of operability during the process design stage. Traditionally the controllabilities of alternate designs are evaluated through simulations. This approach has several drawbacks. First of all the results are biased by the engineer's choice of controller form and parameters. Thus good process designs might be discarded because of the inexperience of the control engineer. Furthermore the results might not be representative because of incorrect choices of operating conditions and disturbances. Finally, especially when a large number of alternatives is to be evaluated, the manpower and computational requirements for the simulation approach are virtually prohibitive and efficient analysis techniques must be used. Morari (1983a) established an appropriate framework which concentrates on identifying plant characteristics that are likely to give rise to control difficulties independent of the selected controller. These characteristics are nonminimum phase behavior, input constraints, and sensitivity to model error.

In this paper we demonstrate that these recently developed techniques allow the efficient and accurate identification of unattractive designs. Further refinements of the original measures are shown to be necessary, however, to evaluate differences among relatively attractive processes. We first review the

Correspondence concerning this paper should be addressed to Manfred Morari, Chemical Engineering, California Institute of Technology, Pasadena, CA 91125.
K. L. Levien is currently at the Chemical Engineering Department, Oregon State University, Corvallis, OR 97331.

derivation of the analytical methods and demonstrate their use with several 3 × 3 models of a distillation system. The true test of any controllability analysis and/or control system design technique is the performance obtained under real-life conditions of industrial complexity. Therefore a pilot plant with two coupled distillation columns for the separation of a ternary mixture of methanol-ethanol-water has been constructed, instrumented, and interfaced with an LSI 11/23 microcomputer. It is shown that the newly developed tools for process resilience analysis are simple to apply, and results are presented for the distillation pilot plant.

Aspects of Resilience

To help clarify and quantify discussions of the process inherent limitation on control performance, Morari (1983a) defined the term "resilience." Qualitatively it describes the ability of a process to move quickly and smoothly from one operating condition to another and to reject disturbances effectively. Because resilience is defined as an inherent property of the process, it is independent of the quality of the controller design. Obviously a process with a poorly designed controller will not follow setpoint changes well or handle disturbances adequately, but this reflects the poor controller design, not the resilience of the process. The insight necessary to remove the bias from the controller design was obtained from the internal model control (IMC) structure (Garcia and Morari, 1982). As shown in Figure 1, the IMC structure is totally equivalent to conventional feedback. Analysis of the IMC structure, however, has led to a deeper understanding of the sources and to quantitative measures of resilience. Ideally, a process is completely resilient; i.e., "perfect" regulatory and servo behavior can be achieved, $[y(t) = y_s(t), \forall t, d]$. Using the IMC structure, Morari and coworkers have shown what process characteristics prevent perfect control from being achieved. There are three limitations on process resilience:

- Nonminimum phase characteristics
- Constraints on manipulated variables
- Sensitivity to model uncertainty

These will be discussed next.

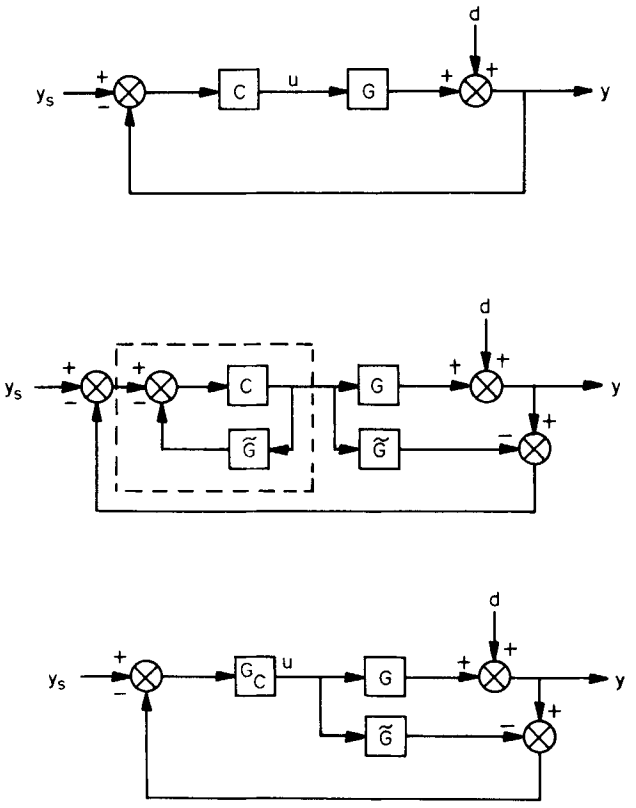

Figure 1. Equivalence of IMC structure to conventional feedback.

Nonminimum phase characteristics

A transfer function containing either time delays or zeros in the right-half complex plane (RHP) is commonly referred to as nonminimum phase (NMP). Holt and Morari (1985a, b) investigated in detail the effect of NMP characteristics on dynamic resilience. For single-input, single-output (SISO) systems the implications of dead time and the relationship between RHP zeros and inverse response are well known. In multiple-input, multiple-output (MIMO) systems, the restrictions imposed by dead times in $\tilde{G}(s)$ on closed-loop performance are more complex. Holt and Morari show that if the matrix of dead times can be arranged by row and column permutations such that the smallest dead time in each row is on the diagonal, then these dead time elements on the diagonal are indicative of the best possible performance achievable for the particular outputs. In addition, for such a distribution of dead times, a decoupled closed-loop response is optimal in the sense of minimum integral squared error (ISE). If the indicated rearrangement is impossible, then a decoupled closed-loop response is no longer ISE optimal.

RHP zeros also restrict the resilience. With the IMC analysis, it has been shown that in the presence of RHP zeros an unstable controller would be required in order to obtain perfect system responses.

Constraints on manipulated variables

All physical process inputs are bounded. These constraints make resilience analysis a nonlinear problem, but insight can still be obtained from linear models when they are properly examined. The singular value decomposition of an appropriately scaled process model will be used to compare limits on disturbance rejection caused by input constraints.

The inputs are assumed to have independent upper and lower constraints

$$\underline{u}_i \le u_i \le \overline{u}_i \tag{1}$$

and are scaled such that

$$|u_i| \le |\underline{u}_i| = |\overline{u}_i| = 1 \tag{2}$$

Thus any input vector with unity Euclidean norm

$$\|u\| \le 1 \tag{3}$$

is feasible. In this paper all transfer function matrices $\tilde{G}(s)$, have been scaled as described and we proceed to analyze which disturbances can be compensated for with $\|u\| \le 1$.

Any complex matrix $\tilde{G}$ can be factored by singular value

decomposition (SVD) into three matrices (Klema and Laub, 1980)

$$\tilde{G} = V\Sigma W^T \tag{4}$$

where Σ = diag $(\sigma_1, \ldots, \sigma_n)$; σ_i = singular value of $\tilde{G}$ ($\underline{\sigma} = \min_i \sigma_i$, $\bar{\sigma} = \max_i \sigma_i$); $\sigma_i > 0$ for the right inverse of $\tilde{G}$ to exist; $V = (v_1, v_2, \ldots)$ = matrix of left singular vectors v_i; and $W = (w_1, w_2, \ldots)$ = matrix of right singular vectors w_i. V and W are unitary, i.e.,

$$V^TV = I, \|v_i\| = 1, \forall i \tag{5a}$$

$$W^TW = I, \|w_i\| = 1, \forall i \tag{5b}$$

From the perfect control postulate

$$y(s) = \tilde{G}(s)u(s) + d(s) = 0 \tag{6}$$

we obtain

$$u = -\tilde{G}^{-1}d = -W\Sigma^{-1}V^Td \tag{7}$$

If we consider all disturbances with unit norm, then $d = v_1$ requires the smallest input.

$$u = -\left(\frac{1}{\sigma_1}\right)w_1 = -\frac{1}{\bar{\sigma}}w_1 \tag{8}$$

and

$$\|u\| = \frac{1}{\bar{\sigma}} \tag{9}$$

For $d = v_n$, the largest input is required.

$$u = -\left(\frac{1}{\sigma_n}\right)w_n = -\left(\frac{1}{\underline{\sigma}}\right)w_n \tag{10}$$

$$\|u\| = \frac{1}{\underline{\sigma}} \tag{11}$$

Thus v_1 will be referred to as the easiest disturbance direction, and v_n as the most difficult direction. If $\underline{\sigma} \approx \bar{\sigma}$, the system is insensitive to the direction of the disturbance. We conclude from Eqs. 10 and 11 that any disturbance with

$$\|d\| < \underline{\sigma}(\tilde{G}) \tag{12}$$

can be handled regardless of its direction. On the other hand Eqs. 8 and 9 show that if

$$\|d\| > \bar{\sigma}(\tilde{G}) \tag{13}$$

then the disturbance cannot be handled, regardless of direction.

The skewness of the feasible disturbance space can be measured by the ratio of the largest and smallest singular values. This is the condition number of $\tilde{G}$ and is denoted as

$$\gamma = \frac{\bar{\sigma}(\tilde{G})}{\underline{\sigma}(\tilde{G})}$$

Thus for a large γ, the feasible disturbance magnitudes in the easiest and the most difficult direction differ widely: the space that can be handled is skewed. When $\gamma = 1$, the feasible disturbance magnitude is independent of direction and equal to the singular values.

The previous discussion focused on analysis of the steady state, $\tilde{G}(0)$. Comparison of $\underline{\sigma}$, $\bar{\sigma}$, and γ for different systems may not be straightforward at times. For example, at low frequencies one process may have a larger $\underline{\sigma}$ than another and thus appear to be more resilient. However at a higher frequency, $\underline{\sigma}$ of the first process may drop below that of the second. In such a case, the frequency content of the disturbances will determine how input constraints restrict resilience.

Making constraints symmetric about the operating point around which the model was identified, and requiring the constraints to be independent introduces conservativeness into the analysis. For example, if an input range of $[-3, +2]$ is scaled as suggested above, only the $[-2, +2]$ range can be considered. Also, since the total distillate flow depends on the boilup, the distillate flow constraint is clearly not independent. Nevertheless the singular values of the model, with the inputs scaled as suggested, provide simple relative measures of the limitations imposed by input constraints and can be interpreted in physical terms.

Sensitivity to model uncertainty

The closed-loop relation for the IMC structure shown in Figure 1 is

$$y = GG_c[I + (G - \tilde{G})G_c]^{-1}(y_s - d) + d \tag{14}$$

The IMC controller (Garcia and Morari, 1985a, b) is

$$G_c = \tilde{G}^{-1}\tilde{G}_+F \tag{15}$$

$\tilde{G}_+$ is a factor chosen to make the controller causal and stable when nonminimum phase characteristics restrict resilience. The IMC filter F is required to make the controller proper and thus realizable, and to make the closed-loop system robust to modeling errors. In the absence of modeling error

$$y = G_+F(y_s - d) + d \tag{16}$$

The closed-loop response is thus specified by the choice of G_+F. Morari and Skogestad (1985) have analyzed the restrictions that have to be placed on G_+F for robust stability. The term robust stability is used to imply that the closed-loop system is stable for some specified family of plants. Multiplicative (L_O and L_I) and additive (L_A) uncertainty descriptions can be used to define different families.

$$G = (I + L_O)\tilde{G} \quad \text{or} \quad L_O = (G - \tilde{G})\tilde{G}^{-1} \tag{17a}$$

$$G = \tilde{G}(I + L_I) \quad \text{or} \quad L_I = \tilde{G}^{-1}(G - \tilde{G}) \tag{17b}$$

$$G = \tilde{G} + L_A \quad \text{or} \quad L_A = (G - \tilde{G}) \tag{17c}$$

Three different families π of plants are obtained by specifying norm bounds on these uncertainties.

$$\pi_O = \{G: \|L_O\| < \ell_O(\omega)\} \tag{18a}$$

$$\pi_I = \{G: \|L_I\| < \ell_I(\omega)\} \tag{18b}$$

$$\pi_A = \{G: \|L_A\| < \ell_A(\omega)\} \tag{18c}$$

Here $\|\cdot\|$ denotes the induced 2-norm of a matrix. The three families define regions of different shape around the nominal plant, so that for multivariable systems the uncertainty descriptions are not equivalent.

A necessary and sufficient condition for robust stability is

$$\det [I + (G - \tilde{G})\tilde{G}^{-1}\tilde{G}_+F] \neq 0 \forall\omega, \forall G \epsilon \pi_A \tag{19}$$

From Eq. 19 a bound on the norm of $\tilde{G}_+F$ can be derived

$$\|\tilde{G}_+F\| < \left[\frac{\|G - \tilde{G}\|}{\|\tilde{G}\|}\right]^{-1} \frac{1}{\gamma(\tilde{G})} \forall G \epsilon \pi_A, \forall\omega \tag{20}$$

which is necessary and sufficient for robust stability if $\tilde{G}_+F$ is diagonal. $\gamma(\tilde{G})$ is the condition number of $\tilde{G}$. The first term on the righthand side has been suggested as a meaningful definition of a relative matrix error. Such a measure is required when model uncertainty cannot be ascribed to individual elements. For perfect control ($\tilde{G}_+F = I$), Eq. 20 yields the requirement

$$\frac{\|G - \tilde{G}\|}{\|\tilde{G}\|} < \frac{1}{\gamma(\tilde{G})} \forall G \epsilon \pi_A, \forall\omega \tag{21}$$

Thus the relative matrix error must be less than the inverse of the condition number of the nominal model for perfect control to be possible. The family π_A, which was defined in Eq. 18c and which appears in Eqs. 20 and 21, is generally conservative in that it often includes a number of plants G that cannot occur in practice. The degree of conservativeness depends on the type of the physical uncertainty and on the scaling of $\tilde{G}$. It is often reasonable to assume that the transfer matrix elements have similar relative errors. Then it can be shown that the scaling which leads to the least conservative definition of π_A is that which makes the absolute values of the elements of $\tilde{G}$ similar. Usually this scaling also minimizes the condition number. These arguments justify the use of the minimized condition number γ^* as a measure of closed-loop sensitivity to model error. This measure is particularly useful when the following two assumptions hold:

1. The scaling that reduces the condition number to γ^* must lead to a tight, i.e., not overly conservative, family, $\pi_{A'}$.

$$\|G_s - \tilde{G}_s\| < \ell_{A'} \tag{22}$$

where $\tilde{G}_s = \tilde{G}$ scaled to minimize γ, $G_s = G$ scaled like $\tilde{G}$.

2. The relative errors $\|G_s - \tilde{G}_s\|/\|\tilde{G}_s\|$ are similar for the different designs to be compared.

For integral control [$\tilde{G}_+F(0) = I$] and for $\omega = 0$, Eq. 19 becomes

$$\det [G(0)\tilde{G}^{-1}(0)] > 0 \quad \forall G \epsilon \pi_A \tag{23}$$

Thus the sign of det [$G(0)$] must be the same for all plants in the family π_A for robust stability with integral control to be possible. This can be regarded as a minimal modeling requirement in order to obtain acceptable performance, at least at the steady state.

Experimental

Equipment

Two pilot plant distillation columns have been modified and linked to form a system that separates a mixture of methanol, ethanol, and water (M, E, W) into three products: the distillate D, side column product S, and bottoms B. The physical arrangement of the columns and peripheral equipment is shown in Figure 2. The copper main column has a 12 in. (30 cm) OD and 19 bubble cap trays. The glass side column has a 6 in. (15 cm) OD and 6 bubble cap trays. Feed location, vapor transfer tray, and liquid transfer tray are selected by manipulated manifold valves for each. Each column has a total condenser and the main column is equipped with a thermosiphon reboiler.

Many alternative distillation configurations can be obtained by selecting different feed, vapor transfer, and liquid return locations. A single configuration, which produces distillate and side products with dominant components of methanol and ethanol, respectively, was selected for the control studies here. Feed is pumped to stage 10 of the main column, vapor is transferred from stage 17 to the side column, and liquid is returned onto stage 18 (with the stages numbered from top to bottom). Nominal operating conditions and products are shown in Table 1.

Measured process outputs are grouped according to their sampling frequency: low, medium, or high. Distillate and side product compositions are calculated every 90 s (low), pressure and temperature are sampled every 2 s (medium). Compositions are measured with a Carle automated gas chromatograph (GC), which contains two thermal conductivity detectors to simultaneously analyze the vapor streams entering the two total condensers. Signals from these detectors are amplified, sent to analog/digital converters, and sampled 5 times/s for peak identification and integration. The mole fraction of water in the bottoms product, b_s, is inferred from the temperature on stage 19, after compensation for pressure.

The process is linked to the computer via a process interface console, which also provides the option of manual control. The process control software package used to implement data acquisition and control is described elsewhere (Levien et al., 1986). The microcomputer used in these experiments was an LSI 11/23 with the RSX-11M operating system.

The coupled distillation columns are controlled via four single-variable control loops and one multivariable control system. The four variables controlled with single loops are feed temperature, liquid level in the bottom of the main column, liquid level in the condensate receiver of the main column, and the pressure difference between the columns. The first loop and manual control of the feed rate fix the feed conditions, the second and third loops maintain liquid holdup in the system, and the last loop is used to maintain vapor flow to the second column. A summary of the loop descriptions is provided in Table 2.

Four process inputs are available for the multivariable control of product compositions: the distillate product flow rate D or the reflux flow rate, R, the steam flow to the reboiler, Q, the vapor flow rate in the vapor transfer line, VT, and the product fraction

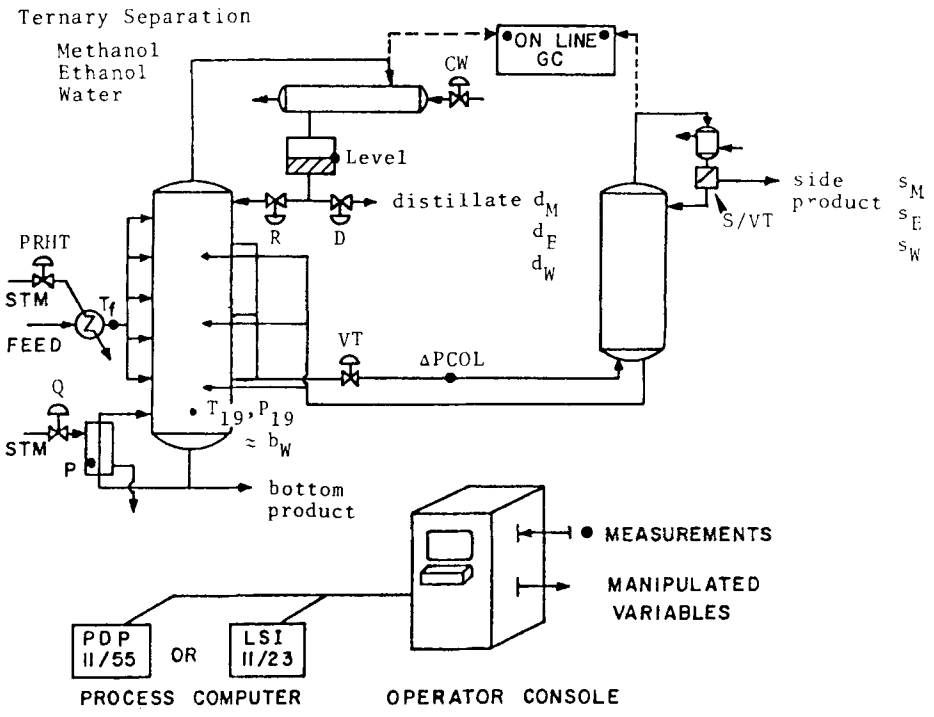

Figure 2. Coupled distillation columns used in experiments.

from the side column, S/VT. In the control experiments of this study, the vapor flow rate control valve, VT, was kept at a fixed opening and two sets of three inputs were compared: $R, Q, S/VT$ vs. $D, Q, S/VT$. The first set is referred to as the conventional set; the second is referred to as the mass balance set. To reduce hysteresis effects, all control valves are equipped with positioners.

Process modeling and system selection

Step response experiments were performed to identify models relating all six product mole fractions measured with the GC and the inferred output b_W, to each input variable of the two sets: $R, Q, VT, S/VT$ and $D, Q, VT, S/VT$. Because multivariable control systems are usually designed to be square, i.e., with the number of manipulated variables equal to the number of controlled outputs, the search for illustrative systems concentrated on square models. Specifying three inputs and outputs creates 1,456 possible systems. Sensitivity to model uncertainty was considered to be one of the most significant factors affecting resilience. Therefore a sensitivity analysis was carried out for 70 physically meaningful candidates and three systems were selected to span an interesting sensitivity range. The chosen systems have either d_M, s_W, b_W or d_M, d_E, s_W as outputs. All inputs and outputs are listed in Table 3.

The transfer matrix elements were assumed to be at most second order, with dead time if necessary. Parameters were determined from a nonlinear least-squares fit to the time domain data. In most cases gains were calculated separately from initial and final steady state outputs. Several inverse responses were observed, as well as underdamped responses. An example response is shown in Figure 3. The complete models for the input sets $D, Q, VT, S/VT$ and $R, Q, VT, S/VT$ are shown in Tables 4 and 5.

From the full models, three 3 × 3 systems were selected for analysis and control experiments. These three, A, B, and C, were chosen to cover a range of steady state γ_s (an approximation of γ^*) values and are shown below.

	Inputs	Outputs
System A	$D, Q, S/VT$	d_M, s_W, b_W
System B	$R, Q, S/VT$	d_M, s_W, b_W
System C	$R, Q, S/VT$	d_M, d_E, s_W

Table 1. Nominal Operating Conditions

Stream	Flow Rate 10^{-5} m^3 · s^{-1} (gpm)	Temp. °C	X_M	X_E	X_W
Feed	3.2 (0.50)	70	0.05	0.05	0.90
Distillate	0.25 (0.040)	60	0.49	0.41	0.10
Side product	0.22 (0.035)	18	0.35	0.49	0.16
Bottoms	2.3 (0.36)	100.8	0.0	0.017*	0.983*

Reflux ratio in main column = 6.8
Reflux ratio in side column = 2.0
Pressure in side column condenser = $P_s < 1.08 \times 10^5$ Pa (15.7 psia)
Pressure in main column (at vapor takeoff) = $P_m = P_s + 0.21 \times 10^5$ Pa (P_s + 3.0 psia)

*Inferred from boiling point after correction for pressure

System A. Process outputs were the mole fraction of methanol in the distillate product, d_M, the mole fraction of water in the side product, s_W, and the mole fraction of water in the bottom product, b_W. Process inputs were the flow rate of distillate products, D, the steam rate sent to the reboiler, Q, and the fraction of vapor transferred to the second column which was recovered as side product, S/VT.

System B. Process outputs were the same as system A. The

Table 2. SISO Control Loops of Coupled Distillation Columns

No.	Task: Maintain	Process Output, y	Manipulated Input, u	Controller
1	Feed conditions	Feed temp., T_f	Steam to preheater	Proportional-integral
2	Main column inventory	Liquid level in bottom of column	Valve in bottom product line	Proportional (mechanical level float)
3	Main column inventory	Main column condensate receiver level	Either reflux rate or distillate product rate in main column	Proportional
4	Vapor flow to second column	Pressure drop in transfer line	Cooling water flow rate to main column condenser	Proportional-integral

first process input, however, was the main column reflux flow rate, R, instead of the distillate product rate.

System C. Process outputs were the mole fraction methanol in the distillate, d_M, the mole fracton ethanol in the distillate, d_E, and the mole fraction water in the side product, s_W. The process inputs were the same as in system B.

The two sets of inputs are referred to as the material balance set D, Q, S/VT and the conventional set R, Q, S/VT. In the identification experiments the amount of vapor sent to the side column, VT, was used as a fourth variable in each set. Thus in the set R, Q, S/VT no manipulated variable was a product flow. Therefore that set of variables does not constitute a material balance system (Shinskey, 1977). The set D, Q, S/VT is a material balance system because the distillate rate is manipulated. In Tables 4 and 5 the inputs have been scaled as discussed previously.

Resilience Analyses of Systems A, B, and C

In this section, the models for the distillation columns will be analyzed and compared for each of the three types of limits to process resilience: nonminimum phase characteristics, constraints on manipulated variables, and sensitivity to model uncertainty.

Nonminimum phase characteristics

In system A only the first output has dead times associated with it. Trivially, system A has the minimum dead time in each row on the diagonal. Therefore decoupled output responses are ISE optional and the only restriction posed by the dead time in the first row is that d_M cannot be changed until after the 8 min. minimum dead time has passed. Systems B and C do not show noticeable dead times. It was determined numerically that no RHP zeros were present in any of the systems. Thus the analysis of nonminimum phase characteristics favors B over A for control of that set of outputs and places no restrictions on the resilience of C.

Table 3. Possible Choices of Variables for Multivariable Control of Coupled Distillation Columns

Inputs		
D	=	Flow rate of distillate product of main column
R	=	Flow rate of reflux returned to main column
Q	=	Steam flow rate to reboiler
VT	=	Flow rate of vapor transferred from main column to side column
S/VT	=	Fraction of vapor sent to side column which is withdrawn as condensed side product
Outputs		
d_M, d_E, d_W	=	Mole fractions of methanol, ethanol, and water in distillate product, measured by GC
s_M, s_E, s_W	=	Mole fractions of methanol, ethanol, and water in side product, measured by GC
b_W	=	Mole fraction of water in bottom product, inferred from temperature on stage 19 adjusted for pressure

Constraints on manipulated variables

Table 6 contains the results of SVD analyses of systems A, B, and C at the steady state. The minimum singular valve ($\underline{\sigma}$) of system A is the largest of the three, system B has the next largest, and system C has the smallest. This implies that system A can handle a larger disturbance than B or C when the direction of the disturbance is unknown. However when $\underline{\sigma}$ values are plotted vs. frequency, as shown in Figure 4, at approximately 0.02 radians/min $\underline{\sigma}$ of system A becomes less than $\underline{\sigma}$ for B and even for C. This suggests that an analysis of steady state information alone can lead to misleading conclusions. During the control experiments presented in this paper we employ IMC filters with bandwidths of 0.14 to 0.56 radians/min. The minimum of $\underline{\sigma}$ for system A lies well within this bandwidth and will therefore affect the closed loop behavior.

From Table 6 values of $\bar{\sigma}$ for A, B, and C seem to be of similar magnitude at steady state. Figure 5 shows that these values are similar up to frequencies of about 0.02 radians/min. At higher frequencies, $\bar{\sigma}$ of system A is approximately one-third that of system B or C. At high frequencies, A is thus somewhat more

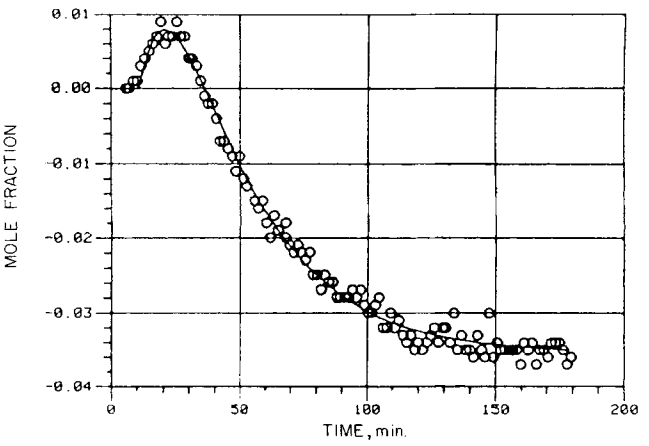

Figure 3. Step response data: response of s_M to increase in Q for input set D, Q, VT, S/VT.

Table 4. Complete Model for Input Set $\{D, Q, VT, S/VT\}$

D	Q	VT	S/VT	
$\frac{-0.117e^{-8s}}{23.1s+1}$	$\frac{0.067e^{-10.5s}}{47.2s+1}$	$\frac{-0.07(-21s+1)}{366s^2+69s+1}$	$\frac{-0.023e^{-71s}}{27.4s+1}$	d_M
$\frac{0.052e^{-8s}}{19.8s+1}$	$\frac{-0.031(-15.8s+1)}{108s^2+63s+1}$	$\frac{0.037(-40s+1)}{845s^2+89s+1}$	$\frac{0.012(-47s+1)}{181s^2+29s+1}$	d_E
$\frac{0.066e^{-8s}}{25.1s+1}$	$\frac{-0.037e^{-8.4s}}{34.3s+1}$	$\frac{0.033(-11.5s+1)}{165s^2+41s+1}$	$\frac{0.011e^{-29s}}{36.8s+1}$	d_W
$\frac{0.098e^{-35s}}{45.9s+1}$	$\frac{-0.041(-20.8s+1)e^{-10.5s}}{367s^2+43.6s+1}$	$\frac{0.056(-7.1s+1)}{3.3s^2+30.8s+1}$	$\frac{-0.087(12.7s+1)}{131s^2+16.6s+1}$	s_M
$\frac{-0.092e^{-27s}}{50.5s+1}$	$\frac{0.031(-33.7s+1)e^{-7s}}{431s^2+44.7s+1}$	$\frac{-0.035e^{-6s}}{33.4s+1}$	$\frac{0.040(8.9s+1)}{118s^2+10.5s+1}$	s_E
$\frac{-0.006(-99s+1)}{1{,}470s^2+47s+1}$	$\frac{0.01}{40.2s+1}$	$\frac{-0.021(-10.4s+1)}{1.3s^2+24s+1}$	$\frac{0.047(48s+1)}{423s^2+52.3s+1}$	s_W
$\frac{0.0725}{890s^2+64s+1}$	$\frac{-0.0029(-560s+1)}{293s^2+51s+1}$	$\frac{0.0068(-43.4s+1)}{193s^2+38s+1}$	$\frac{0.0078}{42.3s+1}$	b_W

restricted than B or C in rejecting disturbances in its easiest direction. From Figure 4 we saw that at high frequencies, A is least restricted in rejecting disturbances in its most difficult direction. By examining γ, the ratio of $\bar{\sigma}$ to $\underline{\sigma}$, as a function of frequency we can see the frequency dependence of the skewness of the space of disturbances that can be handled. Figure 6 is such a plot and shows that at both low and high frequencies the space of disturbances for system A is less skewed than for system B, which is less skewed than for system C. At frequencies around 0.02 radians/min, however, the decrease of $\underline{\sigma}$ in system A causes a dramatic increase in γ(A) so that $\gamma(A) > \gamma(C) > \gamma(B)$. Thus even though an analysis of steady state models shows that system A should be least affected by constraints on its inputs, the analysis of model dynamics indicates that during the adjustments to the disturbance, system A may not be best. Dynamic performance for a specific disturbance depends, of course, on the frequency spectrum of the disturbance.

The easiest and most difficult directions corresponding to steady state values of $\bar{\sigma}$ and $\underline{\sigma}$ are also shown in Table 6. Both the easiest and most difficult directions of system A are similar to those in system B. The easiest directions are characterized by changes of d_M and b_W in opposite directions (one product purer, the other less pure) while s_W remains almost constant. The most difficult directions are changes of d_M and b_W in the same direction (both products purer). These mathematical observations are in complete agreement with qualitative physical intuition. Systems A and B have the same outputs and the same physically feasible values of those outputs, since the only difference between inputs is the use of distillate flow rate instead of reflux flow rate. Thus for these particular systems, it is entirely reasonable that the physical disturbances which cause steady state saturation of the inputs are the same for each system.

In system C the easiest direction is to change the split between methanol and ethanol in the distillate, i.e., to change d_M and d_E in opposite directions. The most difficult direction is to change d_M and d_E in the same direction, i.e., to change the split between

Table 5. Complete Model for Input Set $\{R, Q, VT, S/VT\}$

R	Q	VT	S/VT	
$\frac{0.107(190s+1)}{1{,}550s^2+190s+1}$	$\frac{-0.069(121s+1)}{700s^2+116s+1}$	$\frac{0.262(14.9s+1)}{266s^2+56.6s+1}$	$\frac{0.0065}{62.3s+1}$	d_M
$\frac{-0.042(142s+1)}{1{,}350s^2+145s+1}$	$\frac{0.041(88s+1)}{760s^2+74s+1}$	$\frac{-0.193(11.2s+1)}{162s^2+54.4s+1}$	$\frac{-0.004}{62.3s+1}$	d_E
$\frac{-0.065(199s+1)}{1{,}540s^2+200s+1}$	$\frac{0.028}{5.4s+1}$	$\frac{-0.07(19.6s+1)}{338s^2+57.5s+1}$	$\frac{-0.0025}{67.3s+1}$	d_W
$\frac{-0.07e^{-17s}}{14s+1}$	$\frac{0.034(-5.8s+1)}{68.6s^2+17.7s+1}$	$\frac{0.108(53.8s+1)}{501s^2+77s+1}$	$\frac{-0.096(20s+1)}{171s^2+26s+1}$	s_M
$\frac{0.068e^{-14s}}{19s+1}$	$\frac{-0.046(-7.4s+1)}{25s^2+22.5s+1}$	$\frac{-0.057(94s+1)}{775s^2+120s+1}$	$\frac{0.043(62s+1)}{452s^2+56s+1}$	s_E
$\frac{0.0045(-31s+1)}{290s^2+10.8s+1}$	$\frac{0.013(-13s+1)}{16s^2+32s+1}$	$\frac{-0.052(-13.4s+1)}{61.8s^2+20.4s+1}$	$\frac{0.052}{9.2s+1}$	s_W
$\frac{-0.059}{55.7s^2+20.3s+1}$	$\frac{0.083}{13.5s+1}$	$\frac{-0.017}{22.4s+1}$	$\frac{0.010}{22.1s+1}$	b_W

Table 6. SVD Analysis of Systems A, B, C at Steady State, $\tilde{G}(0)$

	A	B	C
$\bar{\sigma}$	0.152	0.160	0.140
$\underline{\sigma}$	0.030	0.025	0.010
$\gamma = \bar{\sigma}/\underline{\sigma}$, unscaled	5.0	6.5	13.7
$\gamma_s = \tilde{G}$ scaled to reduce $\gamma(\tilde{G})$	3.0	5.9	10.5
	Outputs		
Easiest direction, y_1	$0.137\ d_M$	$0.125\ d_M$	$0.127\ d_M$
	$0.003\ s_W$	$-0.006\ s_W$	$-0.059\ d_E$
	$-0.068\ b_W$	$-0.099\ b_W$	$-0.004\ s_W$
Most difficult direction, y_3	$0.014\ d_M$	$0.014\ d_M$	$0.004\ d_M$
	$-0.001\ s_W$	$-0.010\ s_W$	$0.009\ d_E$
	$0.027\ b_W$	$0.018\ b_W$	$0.000\ s_W$

ethanol and water in the distillate. Since a change in any input variables of system C causes changes in d_M and d_E in opposite directions, it is not surprising that this type of output change requires only small input changes and is therefore "easy." From a physical standpoint, the set of outputs in system C can exhibit nonlinear effects not seen in the outputs of systems A and B. The main column is normally operated at a relatively high reflux ratio, so that an increase in reflux enhances the separation between methanol and ethanol. If the column were operated at a sufficiently low reflux ratio, however, increases in reflux ratio would increase both alcohol mole fractions in the distillate. The sign of the gain between reflux and d_E would be different, and changing d_M and d_E in the same direction would be "easy." This dependence of the easy direction on reflux ratio is due to the highly nonlinear behavior in multicomponent distillation when the mole fraction of a middle component is specified as an output.

Sensitivity to model uncertainty

The use of a scaled condition number has been recommended as a measure of the sensitivity of closed-loop stability to model uncertainty. In that development, the inputs and outputs of $\tilde{G}(s)$ are scaled so that $\gamma(\tilde{G})$ is minimized (γ^*). Because the scaling necessary to minimize γ can not be easily determined, a simple heuristic technique for finding γ_s as an approximation of γ^* is used here. At each frequency $\tilde{G}(i\omega)$ is rescaled to have a maximum amplitude of 1.0 in any row or column. The effect of this scaling at steady state is shown in Table 6. Sensitivity to model uncertainty increases from system A to system B to system C as $\gamma_s(0)$ increases from 3.0 to 5.9 to 10.5. Thus system A is preferred to system B based on this steady state measure, and performance in system C is expected to be very sensitive to model errors.

When γ_s is plotted as a function of frequency, as shown in Figure 7, the ranking changes at intermediate frequencies. Although system C has the largest γ_s for all frequencies, γ_s(A) is greater than γ_s(B) for frequencies near 0.025 radians/min. The original rankings of γ_s are reestablished at higher frequencies. The analysis of process dynamics again indicates that the performance of system A and B should not be expected to be as dissimilar as predicted by the steady state analysis. The control experiments discussed later used filters with bandwidths large enough to include these intermediate frequencies, so that these process characteristics are expected to affect the experimental results.

Grosdidier et al. (1985) have pointed out some interesting

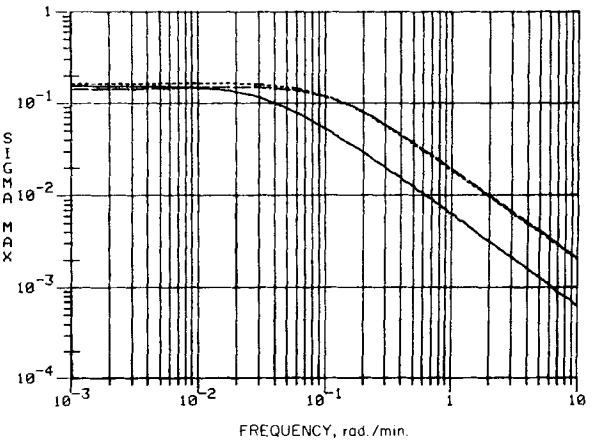

Figure 5. Maximum singular values of systems A, B, C.
—— A; ···· B; ----- C.

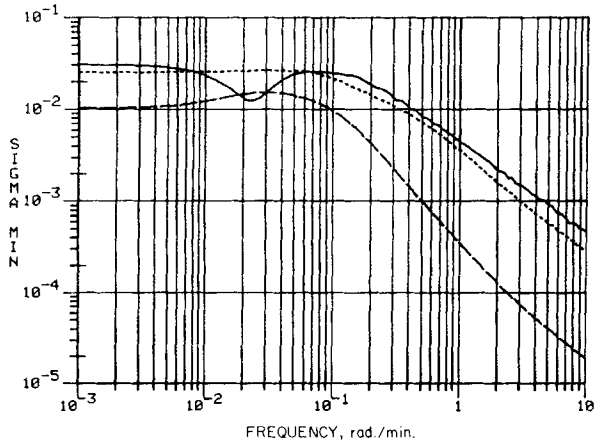

Figure 4. Minimum singular values of systems A, B, C.
—— A; ···· B; ----- C.

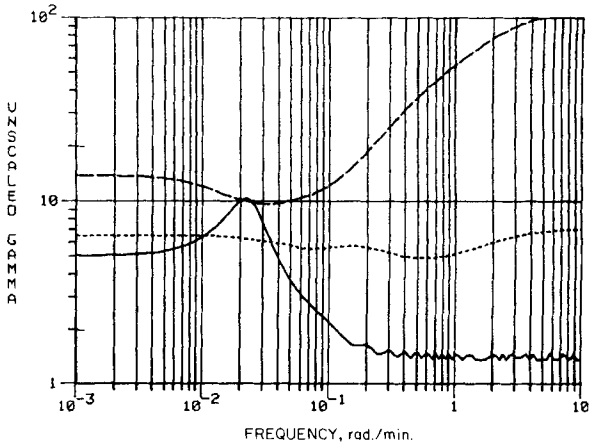

Figure 6. Unscaled condition number γ for systems A, B, C.
—— A; ···· B; ----- C.

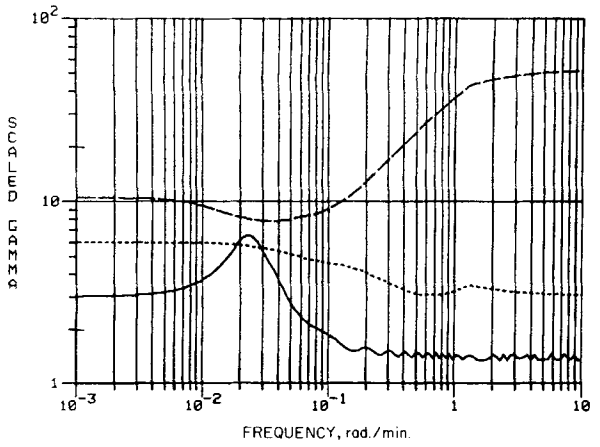

Figure 7. Condition number after scaling γ_s of systems A, B, C.

——— A; · · · · B; ----- C.

connections between sensitivity to plant/model mismatch and the relative gain array (RGA), Λ. They have observed that for 3×3 systems the minimum condition number γ^* obtained by scaling $\tilde{G}$ seems to be bounded by

$$\gamma^* \leq 2 \max \left(\|\Lambda\|_1, \|\Lambda\|_\infty\right) \tag{24}$$

Since the RGA is commonly used to analyze the strength of interactions within the system, this relationship establishes a link between the characterization of interactions and sensitivity to plant/model mismatch. The bounds on γ^* calculated from Eq. 24 are 2.4, 6.0, and 10.2 for systems A, B, and C, respectively, and are thus very similar to the γ_s values. Interactions as measured by the RGA are more severe in system B than in A and are worst in system C.

Case Studies of Plant/Model Mismatch

Two criteria were presented earlier to relate control performance to model accuracy. For a particular case of plant/model mismatch, the inequality in Eq. 20 can be rewritten at steady state as a sufficient condition for the existence of an IMC filter, which makes the closed-loop system stable but eliminates steady state offset $[F(0) = I]$

$$\frac{\|L_A\|}{\|\tilde{G}\|} \gamma_s(\tilde{G}) < 1 \tag{25a}$$

A similar criterion using the input multiplicative uncertainty description is

$$\|L_I\| \gamma_s(\tilde{G}) < 1 \tag{25b}$$

A sufficient condition for instability when the feedback controller contains integral action was given as

$$[\det G(0) \det \tilde{G}(0)] < 0 \tag{26}$$

When this condition holds, then there exists no filter with $F(0) = I$ which makes the closed-loop stable. The criticism of Eqs. 25a, b is that they can be very conservative, i.e., Eqs. 25a, b may not hold, but the closed-loop system might still be stable.

To investigate the conservativeness of the inequality in Eq. 25b the effects of gain errors were studied. Errors in up to five elements were increased until Eq. 25b was violated and then increased further until Eq. 26 was violated. Gains in the plant G were calculated as

$$g_{ij}(0) = \tilde{g}_{ij}(0) + (\alpha_{ij})\rho\tilde{g}_{ij}(0) \tag{27}$$

where $\alpha_{ij} = 1, 0$, or -1 and $\rho \geq 0$. For $\alpha_{ij} = 0$, no error is present in the i, j element of $\tilde{G}$. For $\alpha_{ij} = +1$, the absolute value of the gain of the plant, g_{ij}, is greater than the gain of the model, $\tilde{g}_{ij}$, by a factor of $1 + \rho$. For $\alpha_{ij} = -1$ and ρ less than $+1$, g_{ij} is less than $\tilde{g}_{ij}$ by a factor of $1 - \rho$. For $\alpha_{ij} = -1$ and ρ greater than $+1$, the signs of g_{ij} and $\tilde{g}_{ij}$ are different. A set of α_{ij} values determines a direction of modeling error, and the value of ρ is used to describe the amount of error present. In system A for example let the model be:

$$\tilde{G}(0) = \begin{bmatrix} -0.117 & 0.067 & -0.023 \\ -0.006 & 0.01 & 0.047 \\ 0.0725 & -0.0029 & 0.0078 \end{bmatrix} \tag{28}$$

The three elements with gains of largest absolute value are (1, 1), (3, 1), and (1, 2). Let $\alpha_{11} = \alpha_{31} = \alpha_{12} = 1.0$ and all other $\alpha_{ij} = 0$. For $\rho = 1.0$ in this direction, the plant is

$$G(\rho) = \begin{bmatrix} -0.234 & 0.134 & -0.023 \\ -0.006 & 0.01 & 0.047 \\ 0.145 & -0.0029 & 0.0078 \end{bmatrix} \tag{29}$$

All error directions defined by Eq. 27 with errors in five or less elements were investigated. Figure 8 contains results for systems A, B, and C. For each system, 120 of the possible 121 directions are represented on the abscissas of the plots. In these plots, ρ takes negative as well as positive values. For each direction number, four values of critical ρ are plotted: $\pm\rho$ for violation of Eq. 25b and $\pm\rho$ for violation of Eq. 26. Figure 8 thus presents stability information for 720 distinct cases of plant/model mismatch. If dynamic simulation were used to investigate these stability thresholds, the computational effort would be orders of magnitude larger than the simple analysis presented here. Several observations but only limited conclusions can be made from these and other case studies (Levien, 1985), thus reemphasizing the need for improved analytical tools:

1. Depending on the direction, the difference between the sufficient stability and sufficient instability conditions can be very large. These differences provide some indication of the conservativeness of Eq. 25b.

2. As we move from system A to B to C, in general, smaller perturbations are allowed, as predicted by γ_s comparisons. System A has significantly more insensitive directions, i.e., those where $|\rho| > 2.0$ is required to violate Eq. 26.

3. Various orderings of directions were investigated in an attempt to identify significant error structure, i.e., to see in which elements or combinations of elements errors in gains were most important. Although several interesting patterns were observed, no better general insight was found than that fractional errors in large gains were more important than similar errors in small gains.

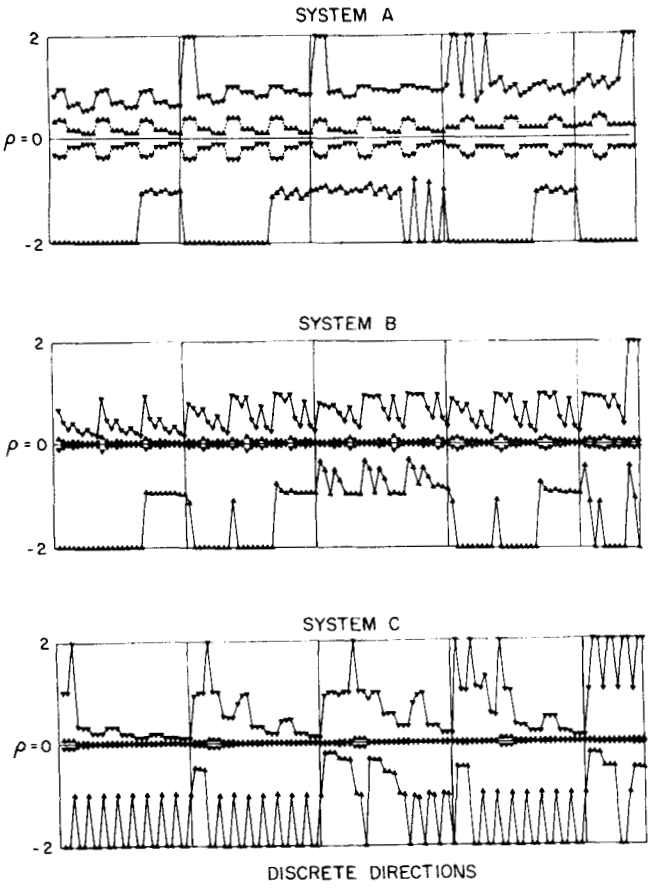

Figure 8. Necessary mismatch ρ to violate sufficient stability or sufficient instability condition.

Experimental Tests of Resilience Predictions

Stability

The initial aspect investigated was sensitivity to model uncertainty. For systems A, B, and C the value of γ_s at steady state was found to be 3.0, 5.9, and 10.5, respectively. Here $\gamma_s[\tilde{G}(0)]$ is the scaled steady state condition number of the transfer function matrix, as discussed previously. From the steady state analysis, the sensitivity to modeling errors was expected to be least in system A, more in system B, and largest in system C. However, an analysis of $\gamma_s(\tilde{G})$ as a function of frequency showed that at frequencies between 0.02 and 0.03 rad/min, $\gamma_s(\tilde{G}_A)$ becomes larger than $\gamma_s(\tilde{G}_B)$. At frequencies above 0.1 rad/min, the steady state ranking is reestablished, but the intermediate frequency behavior indicates that an analysis based solely on steady state information may be misleading.

The IMC controllers designed for these studies include time delay compensation and allow the automatic decoupling of process outputs. The filter form used here was $F = \text{diag}[(\tau_f s + 1)^{-1}]$. Thus there was a single tuning constant, t_f, the time constant of the first-order elements. Each IMC controller G_c was designed as:

$$G_c = \tilde{G}_-^{-1} = \tilde{G}^{-1}\tilde{G}_+ F \tag{30}$$

where $\tilde{G}$ = system model, $\tilde{G}_+$ = a factor of $\tilde{G}$ that makes $\tilde{G}_-^{-1}$ stable and causal, F = IMC filter. The IMC block diagram is shown in Figure 1. The closed-loop relationships in the absence of uncertainty are:

$$y = \tilde{G}_+ F(y_s - d) + d \tag{31}$$

Using the small-gain theorem, a sufficient condition for stability can be derived:

$$\gamma(\tilde{G})\,\|F\|\,\frac{\ell_A}{\|\tilde{G}\|} < 1 \tag{32}$$

where $\gamma(\tilde{G}) = \|\tilde{G}\|\,\|\tilde{G}^{-1}\|$, $\|F\|$ is the norm of the filter, and ℓ_A satisfies $\|G - \tilde{G}\| < \ell_A$.

The filter guarantees robust stability in the presence of model uncertainty. In the limiting case of no uncertainty, the filter time constant is equal to the closed-loop time constant. A larger uncertainty, measured by $\ell_A/\|\tilde{G}\|$, requires a smaller norm of $F(i\omega)$, i.e., a larger filter time constant. The robust stability is obtained by trading off performance, a well-established experience that is explicit in this procedure.

In order to test the steady state ranking of the processes, each control system was first brought to a steady state with constant inputs. The IMC controller was then initiated with a large filter time constant. This filter time constant was reduced by a factor of two in sequential steps until the closed-loop system became unstable, at which point the time constant was increased to reestablish stable control. If stability was not clearly obtained, the time constant was again increased to verify the effect. Thus the following filter time constants, τ_f^*, were found to be sufficient to clearly reestablish stable control:

System	τ_f^* min	Bandwidth rad/min
A	3.6	0.28
B	1.8	0.56
C	14.2	0.07

It was observed that a filter time constant of 0.9 min led to unstable behavior in system A, but that a reduction to 0.5 min was necessary to lead to unstable behavior in system B. The interval between those time constants and the τ_f^* values demonstrates the difficulty in experimentally observing stability limits.

These experimental results agree reasonably well with the theoretical predictions. Assuming the relative errors in the models $\tilde{G}_A$, $\tilde{G}_B$ and $\tilde{G}_C$ to be similar, the experimentally found values for τ_f^* indicate that system C is most sensitive to plant/model mismatch. This confirms the prediction based on $\gamma_s(0)$. On the other hand τ_f^* appears to imply a higher sensitivity of system A than of system B. This contradicts the $\gamma_s(0)$ analysis. A number of reasons could be responsible for this apparent disagreement:

1. A steady state analysis might be insufficient. Recall that the dynamic analysis did not allow to conclude if A or B is less sensitive to model error.

2. The model mismatch might have been larger or in a more "serious" direction for A than for B. Some evidence for a significant error in one of the parameters of $\tilde{G}_A$ was obtained by analysis of the internal model predictions vs. measured outputs during the τ_f^* tests (Levien, 1985).

3. The experimental procedure for τ_f^* might be insufficiently precise.

Reasons (1) and (2) point toward the need for a more refined

resilience analysis technique that allows taking into account frequency dependence and uncertainty structure.

The τ_f^* experiments also showed that the input fluctuation required to maintain the system at a steady state was much larger for system C than for A and B. This agreed with the prediction based on comparisons of $\underline{\sigma}(0)$. Relevant experimental time domain trajectories can be found in Levien (1985).

IMC tuning: robustness vs. performance

The next set of experiments was done to investigate the effects on controller performance in systems A and B when τ_f was increased; i.e., when the IMC controller is tuned on-line. Since a larger τ_f makes the system more robust to mismatch but reduces the inputs to the process, a trade-off of performance for robustness can be anticipated. The same set-point change of +0.04 in $y_1(d_M)$ was made with τ_f equal to either 1.8, 3.6, or 7.1 min. A change in only one set point was made to observe the quality of decoupling achieved by the controller.

System A Tuning. Figure 9 contains the actual and simulated outputs y_1 for filter time constants of 1.8, 3.6, and 7.1 min. As τ_f is increased, the simulated output responded as a first-order system, delayed by the 8 min dead time of $\tilde{G}_+(1, 1)$. In the experiment with the smallest τ_f, significant oscillations appeared in y_1 as it approached the set point. Although this filter time constant was smaller than τ_f^* identified previously, stable control was maintained for this set-point change and a comparison with system B was possible. In experiments with larger τ_f, the initial oscillation disappeared and the output changed more slowly. Significant overshoot occurred in the experiment with the largest τ_f and the response was so sluggish that steady state was not attained after 180 min. Larger τ_f values clearly resulted in slower responses to the set-point change.

Two effects are responsible for differences between the actual and ideal (unconstrained) output responses: mismatch and constraints. Both effects were present when the oscillations in y_1 in the experiment with the smallest τ_f coincided with active constraints. Since y_1 did not settle well, in any experiment even when no constraints were active, model $\tilde{G}_A$ did not appear to be particularly accurate. This conclusion is reinforced when this performance is compared with the results for system B.

System B Tuning. Figure 10 shows the actual and simulated $y_1(d_M)$ outputs for the same series of filter time constants of 1.8, 3.6, and 7.1 min. Here the agreement between the two trajectories was much better than in system A, further evidence that model $\tilde{G}_B$ was a higher quality model than $\tilde{G}_A$. The initial speed and response of y_1 in these experiments are clearly influenced by the τ_f value in the same way as they are when a perfect model is used.

Constraints on Manipulated Variables and Disturbance Rejection. When constraints are placed on the range of inputs that can be implemented, the range of disturbances (or set points) that the system can handle is restricted. With a pure PID controller, input constraints cause integral windup and instability. Special provisions must be built into PID's to prevent this integral or reset windup. Although the IMC structure produces

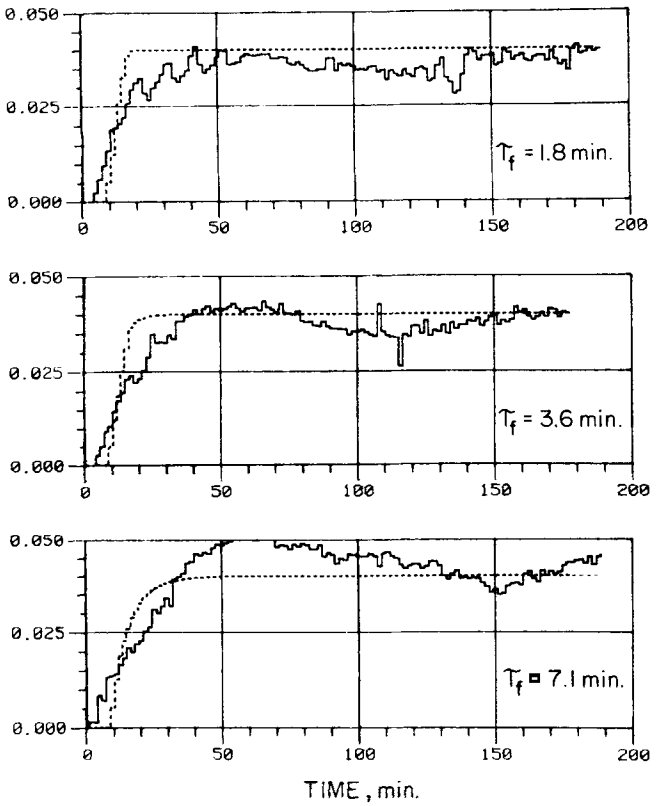

Figure 9. Response of d_M (mol frac) to a set-point change of 0.04 in system A.

—— experiment
····· simulation

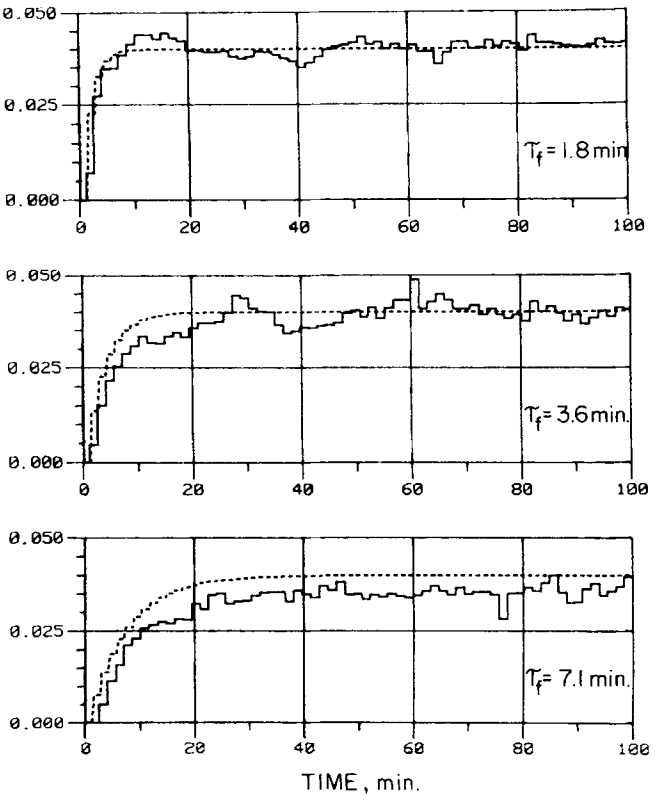

Figure 10. Response of d_M (mol frac) to a set-point change of 0.04 in system B.

—— experiment
····· simulation

integral action when $G_c(0) = \hat{G}^{-1}(0)$, integral windup is avoided automatically when the constrained inputs are used by the model.

To demonstrate the stability of IMC when inputs become constrained and to test disturbance rejection, an experiment was performed during which two consecutive set-point changes in y_1 were made for system B. For this experiment the upper constraint on u_1 was reduced from 1.5 to 1.05 so that a 0.04 set-point change in y_1 was infeasible, i.e., the upper constraint on u_1 would become active.

Figures 11a and 11b respectively show the outputs and inputs for this experiment. As desired, the upper constraint on u_1 was active after approximately 20 min and offset occurred in y_1. During the first 80 min neither y_2 nor y_3 was kept at its set point, although these were attained after 80 min.

At $t = 118$ min, a second set-point change back to the original value was made. Even though u_1 had been constrained for almost 100 min, the IMC controller did not suffer integral windup. Almost immediately after the sign of the y_1 error changed, u_1 was moved off its constraint (errors in y_2 and y_3 were negligible). A disturbance in feed composition was imposed during this set-point change by remixing all of the distillate and side products with some of the bottom product in the feed tank. The feed composition gradually increased in alcohol content during

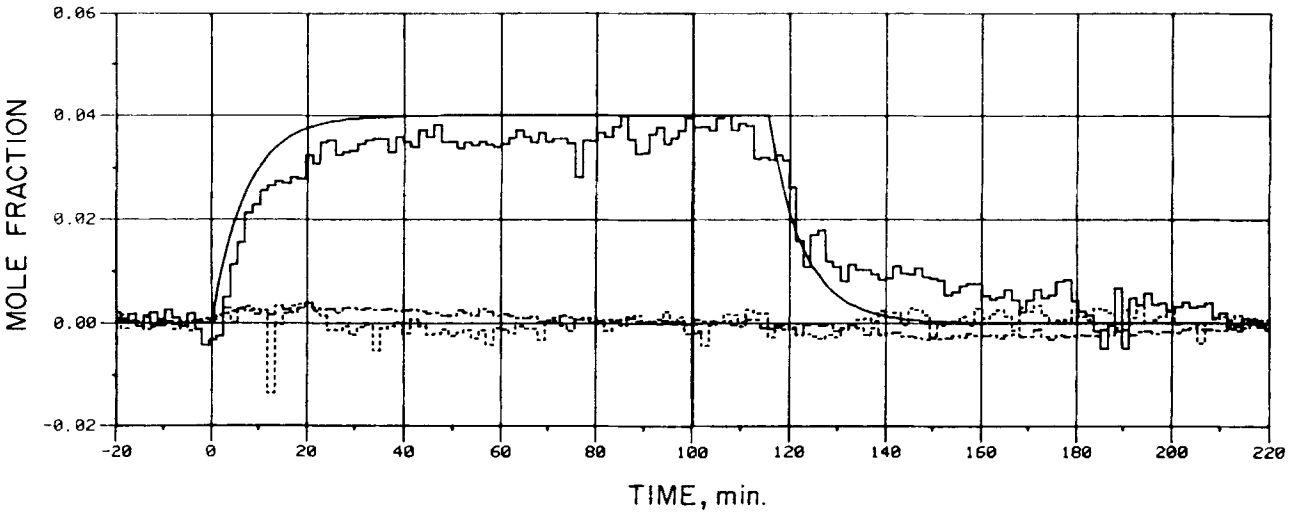

Figure 11a. Responses of outputs in system B during two set point changes.

$t = 0$, y_1 set point changed to 0.04
$t = 118$, y_1 set point returned to 0.00
$t = 120$–135, feed composition changed
——— y_1 (d_M) and simulated y_1
····· y_2 (s_W)
------- y_3 (b_W)

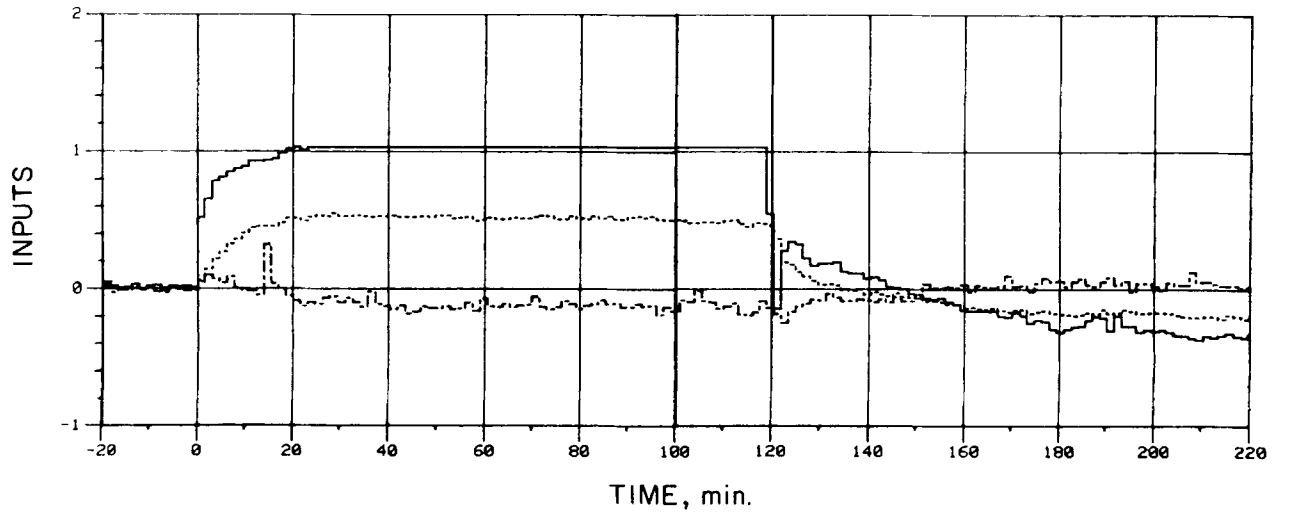

Figure 11b. Inputs to system B during two set point changes in Fig. 6a.

$t = 0$, y_1 set point changed to 0.04
$t = 118$, y_1 set point returned to 0.00
$t = 120$–135, feed composition changed
——— u_1 (D)
····· u_2 (Q)
------- u_3 (S/VT)

the 15 min of this mixing until a new value was established. This change in feed composition changed the input-output relationships and thus changed the plant. Plant/model mismatch was then more significant than during the original set-point change and control during the second set-point change was slightly poorer. Nevertheless, at the end of the experiment the original outputs were attained with new inputs: less reflux and less reboiler steam were required because the feed was richer in alcohol. Thus the IMC controller displayed stable integral action, rapid movement of inputs off active constraints, and good control in the presence of a significant disturbance.

PID Controllers with a Dynamic Decoupler

Recent work by Rivera et al. (1985) with SISO IMC for simple process models has led to new tuning insights for PID controllers. For many simple transfer function models, they show that the IMC design procedure leads to PID controllers, occasionally augmented with a first-order lag. It appeared reasonable to extend these results to multivariable systems when an adequate decoupler can be implemented, which results in a set of simple models on the diagonal of the combined process-decoupler transfer matrix. System B was a relatively accurately known system without dead times, so that a dynamic decoupler design, without the added complexity of dead time compensation, appeared feasible.

Design of a dynamic decoupler

There are several common ways to design a decoupler, D, such that the combined process-decoupler, T, is diagonal

$$\tilde{G}D = T \tag{33}$$

If T is chosen, D can be found as

$$D = \tilde{G}^{-1}T \tag{34}$$

when $\tilde{G}^{-1}$ exists. The decoupler in this study was obtained by specifying each diagonal element of T to be second order, with poles at -0.1 and -0.2 rad/min; this made the decoupler elements proper transfer functions. The model inverse was found by numerically evaluating the inverse at 100 frequencies spaced exponentially between 0.001 and 10 rad/min and approximating the Bode plot of each element with simple transfer functions for frequencies up to about 0.1 rad/min. The fitting was done by inspection by adjusting poles and zeros, since $\tilde{G}(0)^{-1}$ was known. IMC interaction measures (Economou and Morari, 1986) were calculated for the diagonal elements of the decoupled system $\tilde{T}(s) = \tilde{G}(s)D(s)$ and showed that this design for D was effective in removing interactions at least up to 0.1 rad/min.

IMC equivalent PID tuning

The decoupled system T was assumed to consist of three independent SISO systems, each with the transfer function,

$$g(s) = \frac{1}{(10s + 1)(5s + 1)} = \frac{1}{(\tau_1 s + 1)(\tau_2 s + 1)} \tag{35}$$

For Eq. 6 Rivera et al. (1985) propose the controller

$$c(s) = \frac{(\tau_1 s + 1)(\tau_2 s + 1)}{K\epsilon s} = K_c\left(1 + \frac{1}{\tau_I}s + \tau_D s\right) \tag{36}$$

where

$$K_c = \frac{\tau_1 + \tau_2}{K\epsilon s} = 15/\epsilon \tag{37}$$

$$\tau_I = \tau_1 + \tau_2 = 15 \text{ min} \tag{38}$$

$$\tau_D = (\tau_1\tau_2)/(\tau_1 + \tau_2) = 3.33 \text{ min} \tag{39}$$

and ϵ = IMC filter time constant.

The identical diagonal elements of T reduced the multivariable tuning problem to the choice of a single ϵ value, equivalent to the IMC filter τ_f if the approximate inverse were exact. For systems with dead time elements, such as system A, and those with right half-plane transmission zeros, the same restrictions to implementing an inverse when designing an IMC controller will prevent the use of the inverse in the decoupler design. However, the PID tuning procedure is the same regardless of the type of decoupler designed. The IMC-based tuning procedures can be applied to simple approximations of whatever diagonal elements of T are created.

Performance of PID controllers

To test the performance of the decoupler with PID controllers, a set-point change was first performed with parameters equivalent to an IMC filter time constant of 3.6 min. These results were then compared with the performance obtained earlier with IMC. The controller gains were then halved (detuned) to be equivalent to an IMC filter time constant of 7.2 min, and the experiment was repeated.

The performance of the IMC controller, the equivalent PID system, and the detuned PID system is presented in Figure 12. The PID performance is arguably inferior. The two-step procedure of designing a low-order dynamic decoupler and then tuning the parameters of the SISO controllers was less effective than the direct design of the IMC controller. Two problems were found to be inherent in the PID procedure. First, the resultant decoupler was of limited complexity, so that at frequencies above 0.1 rad/min the decoupler's effectiveness decreased. A second aspect was the use of separate discretizations for decoupler and PID algorithms. This was done so that the standard PID algorithms of the control software could be used and the decoupler coefficients were independent of the PID controller parameters. The model error caused by the discretization might have been the reason why a larger filter time constant was required than for IMC for reasonable performance. We conclude that IMC tuning rules for PID's are applicable to a multivariable system when an approximate decoupler is used. If a more complex decoupler (high order and/or a dead time compensator) is required, the robustness, simplicity, and transparency of the IMC structure make IMC an attractive alternative.

Error Detection with Explicit Model

When a multivariable system with significant interactions begins to oscillate, the oscillations will in general appear in all

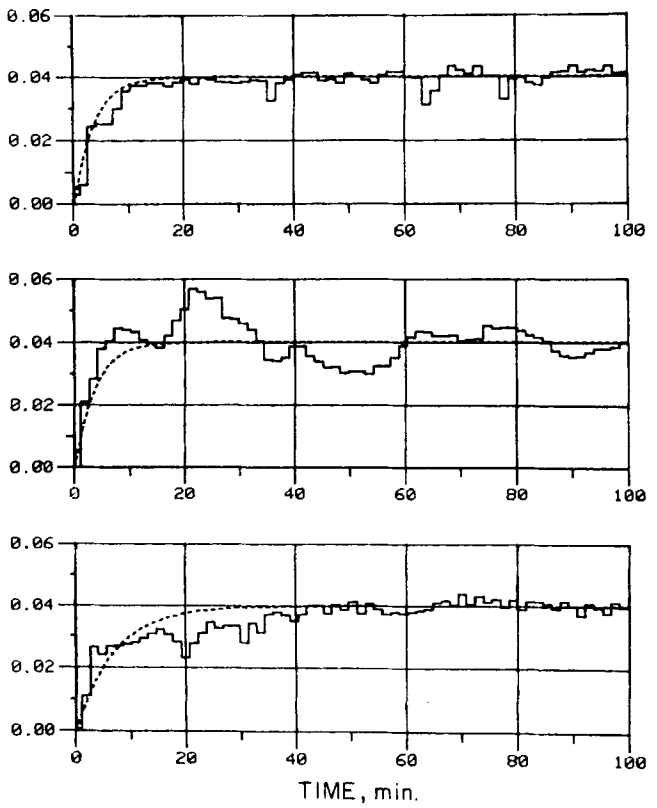

Figure 12. Response of d_M in system B for a set-point change to 0.04 mol frac.

Top, IMC, $\tau_f = 3.6$ min
Middle, PID's, equiv. K_c to $\tau_f = 3.6$ min
Bottom, PID's, equiv. K_c to $\tau_f = 7.2$ min
——— experiment
····· simulation

outputs and all inputs. Since uncertainty in any element of the model can result in instability, it is impossible to localize the source of instability by simply observing process inputs and outputs. In some manner the model used to design the controller must be included in the analysis. The IMC structure provides such an analysis on-line by supplying an explicit value of each modeled output for comparison with the measured value. Thus when modeling error is expected to be the major component of the IMC feedback signal $\tilde{d}$, values of $\tilde{d}_i(t)$ can be used to identify modeling errors for individual outputs. If $\tilde{d}_i(t) \neq 0$, the ith row of $\tilde{G}$ contains modeling error. During the experiment to determine τ_f^* for system A, both $\tilde{d}_2$ and $\tilde{d}_3$ were small, while $\tilde{d}_1$ was large.

The upper plot of Figure 13 contains data taken during that experiment. The measured methanol content in the distillate is shown as a solid curve and the corresponding IMC model output is shown as a dotted curve. Although the model predictions for the other two outputs were found to be fairly accurate, the oscillating values of y_1 from the model can be seen to lag behind those of the plant by 180 degrees. Instability was thus apparently caused by a mismatch in y_1.

Further analysis of Figure 13 was done in an effort to obtain improved stability for an improved model. The average time difference beween plant and model peaks was 6.8 min. It was assumed that a large contribution to the model error was due to the dead time between the distillate rate and d_M, the (1, 1) element of the model. Simulations were performed for plants with smaller dead times in the (1, 1) element. The output behavior was similar to that seen in the tuning studies. Thus the model dead time was revised from 8 to 5 min. To test the effect of this small adjustment, a new controller based on the revised model was designed and tested experimentally for τ_f^*.

The lower plot in Figure 13 displays measured outputs and the corresponding internal model values obtained with the revised model and controller. Oscillations in the output during the second experiment grew much more slowly and were always small. The average time between peaks of measured and calculated outputs was reduced by the amount of adjustment in the model dead time. It thus appears that further decreases in the model dead time may lead to closed loops that are stable for smaller filter time constants.

Model error detection is only one example of the usefulness of the explicit model outputs available with the IMC structure. If a good model is in use but the plant is slowly changing, model adaptation could be performed when an operator is dissatisfied with the model values. If the plant does not change rapidly, explicit model predictions can help operators anticipate the evolution of the process during upsets or operating point changes.

Conclusions

The systems for control studies were chosen to have a range of sensitivities to modeling errors, based on the simplest measure discussed by Morari (1983a): the appropriately scaled, steady state condition number. In order to avoid systems in which good multivariable control is infeasible, systems with significant nonminimum phase characteristics were not selected. From the steady state analyses of the effect of input constraints and the sensitivity of closed-loop stability to model uncertainty, system A, which uses a material balance type control structure, is found to be preferable to system B, which in turn is preferable to system C. From the dynamic analyses of those same restrictions, however, no clear advantage can be claimed for system A. This indicates that a steady state analysis is sufficient to differentiate system C from the other two, but that dynamic models must be analyzed to differentiate between A and B. Thus different resilience indicators (dead times, right half-plane zeros, minimum and maximum singular values, and the condition number) do not consistently favor one system over another when large differences are absent.

Control experiments were designed to challenge these predictions and to illustrate the design and performance of IMC for a complex process. Particular attention was paid to the practical aspects of model uncertainty and input constraints. The resilience analysis was shown experimentally to be sufficient to distinguish between system C, with poor operability, and systems A and B, which could be controlled adequately. It was found, however, that for a ranking of the two better designs, the analysis techniques should include a knowledge of expected control objectives and some estimate of the size and structure of model uncertainty. A useful method to combine the possibly contradictory resilience criteria remains to be found in order to aid the design engineer in making consistent evaluations.

The experiments described here and fully reported elsewhere (Levien, 1985) are some of the most complex distillation control experiments described in the literature to date. The IMC design was shown to be simple to implement and tune for a relatively

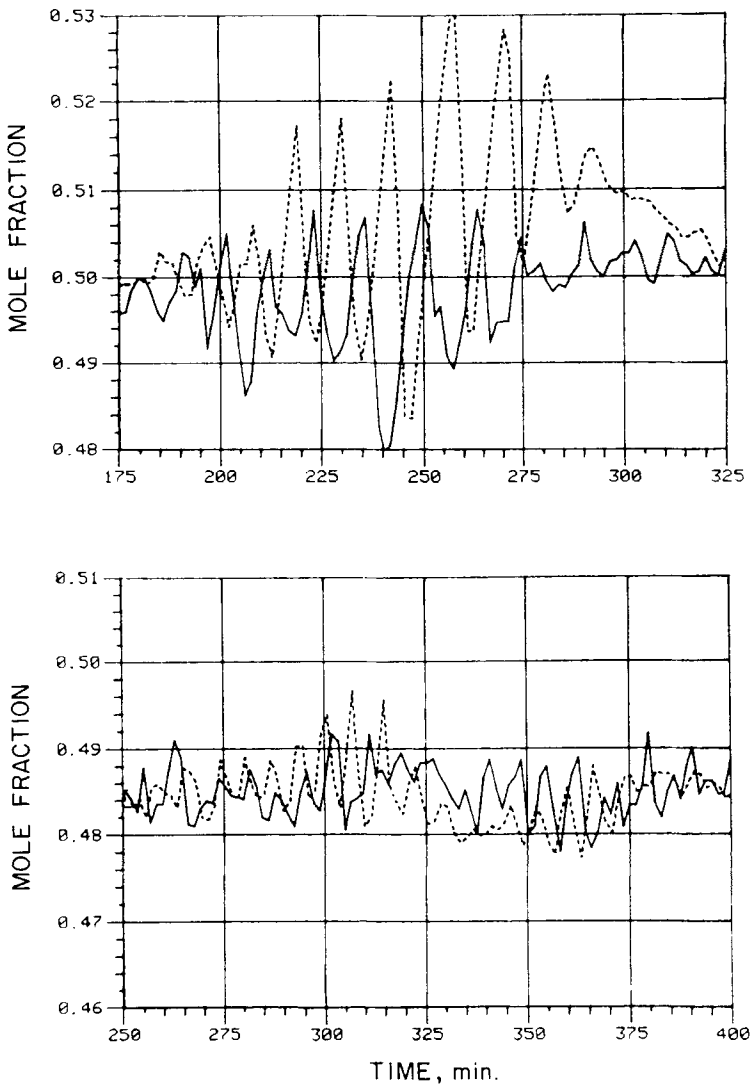

Figure 13. Effect of model change in τ_f^* experiments.

Top, original exp. for τ_f^* in system A
Bottom, τ_f^* exp. done with revised model for system A
——— d_M measurements by GC
····· internal model calculations of d_M

complex multivariable 3 × 3 process. As an alternative procedure to IMC, a dynamic decoupler and three single-input, single-output controllers were also designed and implemented. However, inferior performance was obtained.

Acknowledgment

Financial support from the United States Department of Energy is gratefully acknowledged. The authors wish to thank W. H. Ray for many useful discussions.

Notation

b_i = mole fraction of component i in bottom product
D = distillate flow control valve
$D(s)$ = transfer function matrix of decoupler
d = disturbance to process output
$\tilde{d}$ = feedback signal in IMC structure
d_i = mole fraction of component i in distillate
F = transfer function matrix of IMC filer
G = transfer function matrix of process
g = transfer function of process (SISO)
G_s = transfer function matrix obtained by scaling G similarly to $\tilde{G}_s$
$\tilde{G}$ = transfer function matrix of process model
$\tilde{g}$ = transfer function of process model (SISO)
$\tilde{G}_s$ = transfer function matrix obtained by scaling $\tilde{G}$ to minimize γ
$\tilde{G}_+$ = factor of $\tilde{G}$ (Eq. 15)
G_c = transfer function matrix of IMC controller
I = identity matrix
K = process gain
K_c = controller gain
L_A = additive uncertainty matrix
L_I = input multiplicative uncertainty matrix
L_O = output multiplicative uncertainty matrix
ℓ_A = upper bound on $\|L_A\|$
ℓ_I = upper bound on $\|L_I\|$
ℓ_O = upper bound on $\|L_O\|$
P_m = pressure in mail column at vapor takeoff position
P_s = pressure in side column where vapor feed enters
S = side product flow rate valve
s_i = mole fraction of component i in side product

S/VT = ratio of side product to total condensate in side column
T = transfer function matrix of product of decoupler and process
$\tilde{T}$ = transfer function matrix of product of decoupler and process model
t = time
u = process input(s) as manipulated variable(s)
$\overline{u_i}$ = upper constraint on ith input
$\underline{u_i}$ = lower constraint on ith input
V = matrix of left singular vectors
VT = vapor transfer flow control valve
W = matrix of right singular vectors
y = process output(s)
y_s = setpoint(s)

Greek Letters

α_{ij} = integer used to define mismatch in Eqn. 27
γ = condition number of a matrix
γ_s = condition number of a matrix after scaling the matrix to have elements ≤ 1.0
γ^* = minimum value of γ for a matrix obtained by scaling the matrix
ϵ = time constant of a first order filter
Λ = Relative Gain Array
π_A = family of plants defined with L_A
π_I = family of plants defined with L_I
π_O = family of plants defined with L_O
ρ = measure of extent of mismatch in Eqn. 27
Σ = diagonal matrix of singular values
σ_i = a singular value of a matrix
$\overline{\sigma}$ = the maximum singular value of a matrix
$\underline{\sigma}$ = the minimum singular value of a matrix
τ_f = time constant of a first order filter
τ_f^* = a sufficient experimental τ_f to yield a stable closed loop
ω = frequency

Subscripts

A, B, C = 3×3 systems selected for study
E = ethanol
M = methanol
m = main column
s = side column
W = water

Literature cited

Economou, C., and M. Morari, "Internal Model Control: Multiloop Design," *Ind. Eng. Chem. Process Des. Dev.*, **25,** 411 (1986).

Garcia, C. E., and M. Morari, "Internal Model Control 1," *Ind. Eng. Chem. Process Des. Dev.*, **21,** 308 (1982).

———, "Internal Model Control 2," *Ind. Eng. Chem. Process Des. Dev.*, **24,** 472 (1985a).

———, "Internal Model Control 3," *Ind. Eng. Chem. Process Des. Dev.*, **24,** 484 (1985b).

Grosdidier, P., M. Morari, and B. R. Holt, "Closed-Loop Properties from Steady State Gain Information," *Ind. Eng. Chem. Fundam.* **24,** 221 (1985).

Holt, B. R., and M. Morari, "The Effect of Right Half-plane Zeros on Dynamic Resilience," *Chem. Eng. Sci.*, **40,** 59 (1985a).

———, "The Effect of Deadtime on Dynamic Resilience," *Chem. Eng. Sci.*, **40,** 1229 (1985b).

Klema, V. C., and A. J. Laub, "The Singular Value Decomposition: Its Computation and Some Applications," *IEEE Trans. Auto. Control,* **AC-25,** 164 (1980).

Levien, K. L., "Studies in the Design and Control of Coupled Distillation Columns," Ph.D. Thesis, Univ. Wisconsin, Madison (1985).

Levien, K., C. Chapat, and M. Morari, "RTCP—A Real-Time Control Program for Process Control Research," *Comput. Chem. Eng.* submitted April (1986).

Morari, M., "A General Framework for the Assessment of Dynamic Resilience," *Chem. Eng. Sci.*, **38,** 1881 (1983a).

———, "Robust Stability of Systems with Integral Control," *22nd IEEE Conf. Decision and Control,* San Antonio (1983b).

Morari, M., and S. Skogestad, "Effect of Model Uncertainty on Dynamic Resilience," *PSE '85, Inst. Chem. Eng. Symp. Ser. No. 92,* 493 (1985).

Rivera, D. E., M. Morari, and S. Skogestad, "Internal Model Control: PID Controller Design," *Ind. Eng. Chem. Process Des. Dev.*, **25,** 252 (1986).

Shinskey, F. G. *Distillation Control.* McGraw-Hill, New York (1977).

Manuscript received Aug. 12, 1985, and revision received June 2, 1986.